Effect of viscosity on the dynamics of fission*

K. T. R. Davies
Oak Ridge National Laboratory, Oak Ridge, Tennessee 37830
and Theoretical Division, Los Alamos Scientific Laboratory, University of California , Los Alamos, New Mexico 87545

A. J. Sierk
Kellogg Radiation Laboratory, California Institute of Technology, Pasadena California 91125
and Theoretical Division, Los Alamos Scientific Laboratory, University of California, Los Alamos, New Mexico 87545

J. R. Nix
Theoretical Division, Los Alamos Scientific Laboratory, University of California, Los Alamos, New Mexico 87545
(Received 23 February 1976)

We study the effect of ordinary viscosity on nuclear fission by solving classical equations of motion for the time evolution of fissioning nuclei. The collective potential energy is calculated both by means of the usual liquid-drop model and by means of a modified liquid-drop model that takes into account the lowering in the nuclear macroscopic energy due to the finite range of the nuclear force. The collective kinetic energy is calculated for incompressible, nearly irrotational hydrodynamical flow by use of the Werner-Wheeler method. The Rayleigh dissipation function, which describes the transfer of energy of collective motion into internal excitation energy, is calculated under the assumption that nuclear dissipation arises from individual two-body collisions. Prior to scission the nuclear shape is specified in terms of smoothly joined portions of three quadratic surfaces of revolution. After scission the fission fragments are represented by two spheroids with collinear symmetry axes. In addition to slowing the system down and converting some of the collective energy into internal energy, two-body viscosity hinders the formation of a neck. This leads to a more elongated scission configuration and consequently to a smaller final fission-fragment kinetic energy. From a comparison of calculated and experimental most probable fission-fragment kinetic energies for nuclei throughout the periodic table, we determine that at high excitation energies the average value of the viscosity coefficient μ is $\mu = 0.015 \pm 0.005$ TP $= 9 \pm 3\times10^{-24}$ MeV s/fm^3, provided that nuclear dissipation arises from two-body collisions. This is about 30% of the value that is required to critically damp the quadrupole oscillations of idealized heavy actinide nuclei.

[NUCLEAR REACTIONS, FISSION Calculated dependence of most probable fission-fragment kinetic energies on viscosity and compared with experimental values. Liquid-drop model, hydrodynamical model, nuclear potential energy of deformation, nuclear inertia, nuclear dissipation, numerical solution of classical equations of motion for fissioning nuclei.]

I. INTRODUCTION

In studying the dynamics of large-scale nuclear shape changes such as occur in fission and heavy-ion reactions, one may use either a microscopic approach or a macroscopic approach. In a microscopic approach one starts with a given interaction between nucleons and solves the time-dependent many-body Schrödinger equation in some approximation. By use of simple effective interactions and the time-dependent Hartree-Fock approximation this has been done recently for some special cases involving the collision of two slabs of nuclear matter[1] and the collision of two relatively light nuclei.[2,3] Such calculations are promising, but the full realization of their possibilities still requires several extensions. These include considering much heavier nuclear systems, using more realistic nucleon-nucleon potentials, incorporating residual interactions, allowing for mass-asymmetric and axially asymmetric deformations, and improving the type of wave function considered.

In a macroscopic approach one starts with a continuous distribution of matter that is subjected to given forces and solves the resulting equations of motion in some approximation. Although one usually starts directly with a specific macroscopic model, it is alternatively possible by use of various approximations to derive macroscopic equations from the time-dependent many-body Schrödinger equation.[4-9]

Once obtained, macroscopic equations of motion may be solved either directly by use of numerical methods,[10-12] or alternatively by parametrizing the nuclear shape in some way, which leads to a set of coupled nonlinear differential equations that is in turn solved numerically.[13-28] Both because of its relative simplicity and because it permits concentrating on a few essential degrees

of freedom, this latter method has been widely used in the study of fission dynamics. This method also permits incorporating into an otherwise macroscopic model certain purely microscopic effects. These include single-particle corrections to the nuclear potential energy of deformation,[25-28] and nuclear inertias that are larger than irrotational values.[29-31]

Irrespective of the precise approach that is taken, a problem of central importance in large-scale nuclear shape changes is nuclear dissipation. This is the transfer of energy from collective degrees of freedom which describe the overall geometrical shape of the nucleus to internal degrees of freedom which describe the motion of the nucleons relative to this fixed shape. In a purely microscopic calculation, where the dissipation is determined automatically through the solution of the time-dependent many-body equations, one need not make this separation into collective and internal coordinates. Unfortunately, because of the complexity and time reversibility of the solution, it is difficult in a purely microscopic approach to gain insight into the basic mechanism of nuclear dissipation.

At issue is whether nuclear dissipation proceeds primarily by means of individual two-body collisions, as in the case of ordinary fluids, or by means of nucleons colliding with a moving potential wall.[32-35] Until recently it has always been taken for granted that nuclear dissipation is of the ordinary two-body type,[19-21,36-39] and it is this type of viscosity that we consider here.

In retrospect, one might argue that ordinary two-body viscosity should apply only to systems for which the collision mean free path is small compared to the spatial dimensions. In nuclei, where the collision mean free path is larger than the nuclear diameter, the alternative one-body dissipation mechanism of nucleons colliding with a moving potential wall might be expected to apply. Some recent calculations[35] in fact confirm that most probable fission-fragment kinetic energies of nuclei throughout the Periodic Table are reproduced equally well with a large one-body dissipation as with the two-body viscosity considered here. In order to decide between these two alternatives, it is crucial to know the consequences of each, and it is in this spirit that we describe our present calculations based on ordinary two-body viscosity.

In our study of nuclear dynamics we use a macroscopic approach in which the nuclear shape is parametrized in a simple way. We restrict our attention to nuclei at high excitation energies, where single-particle effects are expected to become relatively small. This permits us to calculate the collective potential energy in terms of the liquid-drop model, or alternatively in terms of a modified liquid-drop model that takes into account the lowering in the nuclear macroscopic energy due to the finite range of the nuclear force.[20-22,40,41] Because of the high excitation energies and the large distortions encountered in fission, the collective kinetic energy should be much closer to the incompressible, irrotational value than for nuclei in their ground states.[20] As an approximation to incompressible, irrotational flow we use the Werner-Wheeler method, which determines the flow in terms of circular layers of fluid.[17,23,42]

Under the assumption that nuclear dissipation arises from two-body collisions, we calculate the transfer of energy of collective motion into internal excitation energy in terms of the Rayleigh dissipation function.[43] The presence of dissipation introduces terms that are linear in the collective velocities into the equations of motion. For a given set of initial conditions, these equations are solved numerically for the time evolution of the generalized coordinates that describe the shape and their conjugate momenta. These points are discussed in Sec. II. Section III contains the results of our calculations, including a comparison with experimental most probable fission-fragment kinetic energies for the fission of nuclei throughout the Periodic Table. This is in an attempt to determine the average value of the two-body viscosity coefficient at high excitation energies. In Sec. IV we summarize our results and present our conclusions.

II. THEORY

We obtain and solve classical equations of motion for fissioning nuclei under the assumption that the nucleus is an incompressible fluid whose hydrodynamical flow is nearly irrotational. In the presence of viscosity the actual flow is of course no longer irrotational. However, the assumption of a specific type of hydrodynamical flow allows us to take viscosity into account by means of the Rayleigh dissipation function, which is defined as one-half the rate at which energy is transferred from collective to internal degrees of freedom. This procedure leads to the generalized Lagrange or Hamilton equations.[43]

The criterion for the validity of a classical treatment is that, for a given degree of freedom, the de Broglie wavelength be small compared to the distance over which the potential energy changes appreciably. This condition is well satisfied for the fission degree of freedom so long as the kinetic energy in the fission direction is great-

er than about 1 MeV.

In the present treatment shell and pairing corrections[44] are neglected entirely. Thus, we restrict ourselves to cases in which the excitation energy is sufficiently high to effectively destroy the single-particle corrections; the system then responds mainly to the dominant macroscopic contributions. This treatment of course limits us to cases in which the most probable mass division is symmetric.

A. Potential energy

The potential energy of a deformed nucleus is given by

$$V = E_{\rm nm} - E_{\rm nm}^{(0)} + E_{\rm C} - E_{\rm C}^{(0)} , \tag{1}$$

where $E_{\rm nm}$ is the nuclear macroscopic energy and $E_{\rm C}$ is the Coulomb energy. The quantities $E_{\rm nm}^{(0)}$ and $E_{\rm C}^{(0)}$ are the corresponding energies for a spherical shape. As the nucleus deforms, its volume is assumed to remain equal to $\frac{4}{3}\pi R_0^3$, where

$$R_0 = r_0 A^{1/3}$$

is the radius of the sphere.

The Coulomb energy is given by

$$E_{\rm C} = \tfrac{1}{2}\rho_e^2 \int\int \frac{d^3r_1 d^3r_2}{|\vec{r}_1 - \vec{r}_2|} , \tag{2}$$

where

$$\rho_e = Ze/(\tfrac{4}{3}\pi R_0^3) \tag{3}$$

is the constant charge density. For a spherical shape Eq. (2) reduces to

$$E_{\rm C}^{(0)} = \tfrac{3}{5} Z^2 e^2/R_0 = a_{\rm C} Z^2/A^{1/3} , \tag{4}$$

while for a nucleus of arbitrary axially symmetric shape the Coulomb energy is calculated efficiently by use of Gaussian-Legendre quadrature formulas.[45] It is convenient to define the relative Coulomb energy B_C by means of the relationship

$$E_{\rm C} = B_{\rm C} E_{\rm C}^{(0)} . \tag{5}$$

We consider two types of nuclear macroscopic energies. The first is the usual surface energy of the liquid-drop model, which we write as

$$E_s = B_s E_s^{(0)} . \tag{6}$$

The quantity B_s is the relative surface energy and $E_s^{(0)}$ is the spherical surface energy, which is given by

$$E_s^{(0)} = a_s\{1 - \kappa[(N-Z)/A]^2\} A^{2/3} , \tag{7}$$

where a_s is the surface-energy constant and κ is the surface-asymmetry constant.[46] The relative surface energy B_s is therefore equal to the surface area of the deformed shape divided by $4\pi R_0^2$. Upon substituting Eqs. (5) and (6) into (1) we obtain

$$V = [(B_s - 1) + 2x(B_{\rm C} - 1)] E_s^{(0)} , \tag{8}$$

where

$$x = \frac{E_{\rm C}^{(0)}}{2E_s^{(0)}} = \frac{Z^2/A}{(2a_s/a_{\rm C})\{1 - \kappa[(N-Z)/A]^2\}} \tag{9}$$

is the fissility parameter. Although deficient in some respects,[44] the values of the constants presented by Myers and Swiatecki at the 1966 Lysekil symposium[46] are frequently used for calculating x and $E_s^{(0)}$.

The second type of nuclear macroscopic energy that we use is obtained from a double volume integral of a Yukawa effective two-body potential, i.e.,[20-22,40,41]

$$E_{\rm nm} = -\frac{\beta}{4\pi a^3} \int\int \frac{e^{-|\vec{r}_1 - \vec{r}_2|/a}}{|\vec{r}_1 - \vec{r}_2|/a} d^3r_1 d^3r_2 , \tag{10}$$

where β measures the strength of the interaction and a is the range of the Yukawa potential. This expression takes into account the finite range of the nuclear force, which is very important for describing the formation of the neck in fission and for describing two nearly touching nuclei in heavy-ion reactions. For a spherical shape Eq. (10) reduces to

$$E_{\rm nm}^{(0)} = \beta[-\tfrac{4}{3}\pi R_0^3 + 2\pi a R_0^2 - 2\pi a^3 + 2\pi a(R_0 + a)^2 \exp(-2R_0/a)] . \tag{11}$$

These finite-range energies contain a constant volume energy $-\frac{4}{3}\pi\beta R_0^3$, but this term cancels when Eq. (11) is subtracted from Eq. (10) to obtain the nuclear macroscopic energy relative to the spherical shape. The remaining shape-dependent terms include the usual surface energy of the liquid-drop model plus some finite-range terms which vanish as the Yukawa range a approaches zero. The values of the constants in Eqs. (4) and (11) are obtained from analyses of electron-scattering experiments[47,48] and from adjustments to experimental fission-barrier heights and heavy-ion interaction-barrier heights.[40] The integrals in Eq. (10) are evaluated efficiently for axially symmetric shapes by use of the same Gaussian-Legendre quadrature method that is used to calculate the Coulomb energy.[45]

B. Kinetic energy and dissipated energy

Under certain restrictions that are discussed in Appendix A, the collective kinetic energy of the system depends quadratically on the general-

ized velocities. i.e.,

$$T=\frac{1}{2}\sum_{i,j} M_{ij}(q)\dot{q}_i\dot{q}_j \ , \tag{12}$$

where

$$q\equiv q_1, q_2, \ldots, q_N$$

denotes the N generalized coordinates that specify the shape of the system, and where time differentiation is denoted by a dot. The shape dependence of T is contained in the elements $M_{ij}(q)$ of the inertia tensor.

Frictional forces are introduced by means of the Rayleigh dissipation function[43]

$$F=\frac{1}{2}\sum_{i,j} \eta_{ij}(q)\dot{q}_i\dot{q}_j \ , \tag{13}$$

where $\eta_{ij}(q)$ denotes an element of the shape-dependent viscosity tensor. The rate of dissipation of collective energy into internal excitation energy is equal to $2F$.

In Appendix A we show how to evaluate the inertia and viscosity tensors for an incompressible, nearly irrotational fluid by use of the Werner-Wheeler method.[17,23,42] The accuracy of this method for describing viscous flow is discussed in Appendix B.

C. Equations of motion

The classical equations of motion, including dissipative effects, are the generalized Lagrange equations[43]

$$\frac{d}{dt}\left(\frac{\partial L}{\partial \dot{q}_i}\right)-\frac{\partial L}{\partial q_i}=-\frac{\partial F}{\partial \dot{q}_i}, \quad i=1,2,\ldots,N \ , \tag{14}$$

where

$$L(q,\dot{q})=T(q,\dot{q})-V(q) \tag{15}$$

is the Lagrangian for the system. Upon substituting Eqs. (12), (13), and (15) into Eq. (14) and using the symmetry of the inertia and viscosity tensors, we obtain

$$\sum_j M_{ij}(q)\ddot{q}_j+\sum_{j,k}\left[\frac{\partial M_{ij}(q)}{\partial q_k}-\frac{1}{2}\frac{\partial M_{jk}(q)}{\partial q_i}\right]\dot{q}_j\dot{q}_k + \sum_j \eta_{ij}(q)\dot{q}_j+\frac{\partial V(q)}{\partial q_i}=0, \quad i=1,2,\ldots,N \ , \tag{16}$$

a system of N coupled nonlinear second-order differential equations.

It is sometimes convenient to use the Hamiltonian formulation of the classical equations of motion. We first define the generalized momenta and Hamiltonian function H in the usual way by[49]

$$p_i=\frac{\partial L}{\partial \dot{q}_i}=\sum_j M_{ij}(q)\dot{q}_j, \quad i=1,2,\ldots,N \ , \tag{17}$$

and

$$H(q,p)=\sum_i \dot{q}_i p_i - L(q,\dot{q}) \ . \tag{18}$$

Then the generalized Hamilton equations, including dissipative effects, are

$$\dot{q}_i=\frac{\partial H}{\partial p_i}=\sum_j [M(q)^{-1}]_{ij}p_j, \quad i=1,2,\ldots,N \ , \tag{19a}$$

and

$$\dot{p}_i=-\frac{\partial H}{\partial q_i}-\frac{\partial F}{\partial \dot{q}_i} =-\frac{1}{2}\sum_{j,k}\frac{\partial [M(q)^{-1}]_{jk}}{\partial q_i}p_j p_k -\sum_{j,k}\eta_{ij}(q)[M(q)^{-1}]_{jk}p_k-\frac{\partial V(q)}{\partial q_i}, \quad i=1,2,\ldots,N, \tag{19b}$$

a system of $2N$ coupled nonlinear first-order differential equations. In our work we integrate numerically Eqs. (19) by use of a fourth-order Adams-Moulton predictor-corrector method,[50] with the starting procedure based on a modified fourth-order Runge-Kutta method.[50,51]

As discussed in Appendix A, the viscosity tensor η is proportional to the viscosity coefficient μ. It is of interest to study the dynamical equations of motion for the limiting case of infinite viscosity. As $\mu\to\infty$ the time required to undergo a finite displacement also becomes infinite. This makes it convenient to define the quantities

$$t'=t/\mu$$

and

$$\eta'_{ij}=\eta_{ij}/\mu \ ,$$

which remain finite as $\mu\to\infty$. In this limit Eq. (16) reduces to

$$\frac{dq_i}{dt'}=-\sum_j [\eta'(q)^{-1}]_{ij}\frac{\partial V}{\partial q_j}, \quad i=1,2,\ldots,N \ , \tag{20}$$

a system of N coupled nonlinear first-order differential equations which is integrated numerically as indicated above.

D. Deformation coordinates

We restrict ourselves to axially symmetric nuclei and describe the shape of a fissioning nucleus prior to scission in terms of smoothly joined portions of three quadratic surfaces of revolution.[17] The results reported here are also restricted to reflection-symmetric nuclei, which

means that we consider explicitly only three deformation coordinates. These specify (1) the distance between the centers of the two end spheroids that form the shape, (2) the eccentricity of these end spheroids, and (3) the eccentricity of the middle quadratic surface that forms the neck.

For displaying the dynamical paths of fissioning nuclei it is convenient to project out of this three-dimensional space (or in general out of an infinite-dimensional space) the two most important symmetric degrees of freedom. These are defined conveniently in terms of the central moments[19,20,52]

$$r = 2\langle z \rangle \tag{21a}$$

and

$$\sigma = 2\langle (z - \langle z \rangle)^2 \rangle^{1/2} , \tag{21b}$$

where the angular brackets $\langle\ \rangle$ denote an average over the half volume to the right of the midplane of the reflection-symmetric shape. The moment r gives the distance between the centers of mass of the two halves of the dividing nucleus, and σ gives a measure of the elongation of each half about its center of mass.

For small distortions about a spherical shape the moments r and σ are easily related to the coordinates α_2 and α_4 in an expansion of the system's radius vector in Legendre polynomials. To first order this relationship is

$$r = \tfrac{3}{4}(1 + \alpha_2 - \tfrac{1}{6}\alpha_4)R_0$$

and

$$\sigma = (\tfrac{19}{80})^{1/2}(1 + \alpha_2 + \tfrac{15}{38}\alpha_4)R_0 .$$

For a pure spheroidal distortion, r and σ are given exactly by

$$r = \tfrac{3}{4}c$$

and

$$\sigma = (\tfrac{19}{80})^{1/2}c ,$$

where c is the semisymmetry axis of the spheroid.

The three-quadratic-surface parametrization is used to study the dynamical motion of the system from its saddle point to scission. After scission the fission fragments are described in terms of two separated spheroids.[13,14] The transition from one shape parametrization to the other is accomplished by equating the values of r and σ and the corresponding velocities $\dot{r}$ and $\dot{\sigma}$ before and after scission. This introduces a small but nevertheless tolerable discontinuity in the various contributions to the total energy.

For two equal separated spheroids r is equal simply to the distance between their centers, and σ is given by

$$\sigma = \frac{2}{\sqrt{5}}c_1 ,$$

where c_1 is the semisymmetry axis of one of the spheroids. For such postscission shapes the inertia tensor and viscosity tensor are both diagonal with respect to the moments r and σ.

The division of the total energy release into translational kinetic energy and excitation energy of the fission fragments at infinity is determined by integrating the postscission equations of motion until the higher multipole corrections to the Coulomb interaction energy are negligible. At this point the sum of the translational kinetic energy and the Coulomb interaction energy is taken to be the final fission-fragment kinetic energy at infinity. The excitation energy is obtained finally by subtracting the kinetic energy from the total energy released in going from the saddle point to infinity.

III. CALCULATED RESULTS

We have used the methods described in the preceding section to calculate the effect of two-body viscosity on various aspects of nuclear fission. We present first our results concerning the induced fission of the compound nucleus ^{236}U, and second our results concerning the spontaneous fission of ^{252}Cf. This is followed by a discussion of the fission of nuclei throughout the Periodic Table. In the final part of this section we compare our calculated most probable fission-fragment kinetic energies with experimental values for the fission of nuclear systems ranging from ^{80}Sr to ^{278}110. Provided that nuclear dissipation arises from two-body collisions, this permits us to determine the average value of the two-body viscosity coefficient at high excitation energies.

A. Induced fission of ^{236}U

As an example pertinent to induced fission, we consider a ^{236}U compound nucleus that is started in motion at its macroscopic saddle point with 1 MeV of kinetic energy in the fission direction. (For heavy nuclei the dependence of the fission eigenvector upon viscosity is so slight that we may safely use the eigenvector calculated for zero viscosity.) The nuclear macroscopic energy is calculated in terms of a double volume integral of a Yukawa function.

Figure 1 illustrates the effect of two-body viscosity on the dynamical descent from the saddle point to scission. The unit of viscosity is the terapoise, which is given by

$$1\ \mathrm{TP} = 10^{12}\mathrm{P} = 10^{12}\ \mathrm{dyn\ s/cm^2}$$
$$= 6.24 \times 10^{-22}\ \mathrm{MeV\ s/fm^3} = 0.948\ \hbar/\mathrm{fm^3} .$$

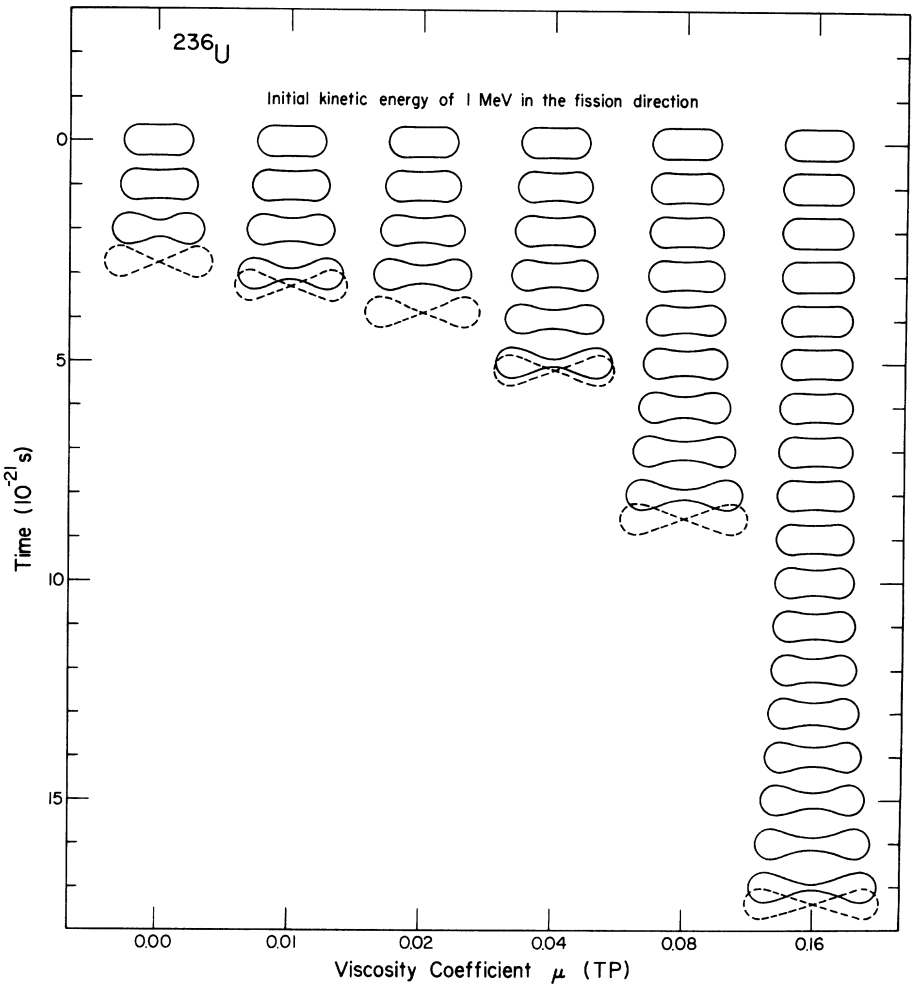

FIG. 1. Calculated shapes at equal time intervals of a ^{236}U nucleus from its macroscopic saddle point to scission, for various values of the two-body viscosity coefficient μ. The initial conditions in each case correspond to starting from the saddle point with 1 MeV of kinetic energy in the fission direction. The scission shapes are shown dashed.

For a viscous system some of the decrease in collective potential energy is converted into internal excitation energy rather than into collective kinetic energy. This causes the system to slow down, as can also be seen in Fig. 2. For an initial kinetic energy of 1 MeV in the fission direction, the time from saddle to scission increases from 2.8×10^{-21} s for zero viscosity to 17.3×10^{-21} s for $\mu = 0.16$ TP. An increase in the initial kinetic energy in the fission direction decreases the time from saddle to scission and vice versa, especially for small values of viscosity.

A viscous ^{236}U nucleus therefore undergoes scission with less translational kinetic energy than a nonviscous one. But, in addition, the scission configuration is more elongated for a viscous ^{236}U nucleus than for a nonviscous one. This is because in the presence of viscosity the dynamical path readjusts itself so as to lessen the energy dissipation. The large gradients in the hydrodynamical flow pattern during neck formation lead to a large dissipation for this mode, which is therefore hindered. In the fission of a heavy viscous nucleus, both the smaller translational kinetic energy at scission and the more elongated scission configuration decrease the final translational kinetic energy of the fission fragments at infinity.

In Fig. 3 we show the dynamical paths for ^{236}U for several values of viscosity projected onto the two-dimensional space of center-of-mass separation r and fragment elongation σ. Although the initial conditions correspond to starting from the saddle point with 1 MeV of kinetic energy in the fission direction, the most probable dynamical paths corresponding to starting from rest an in-

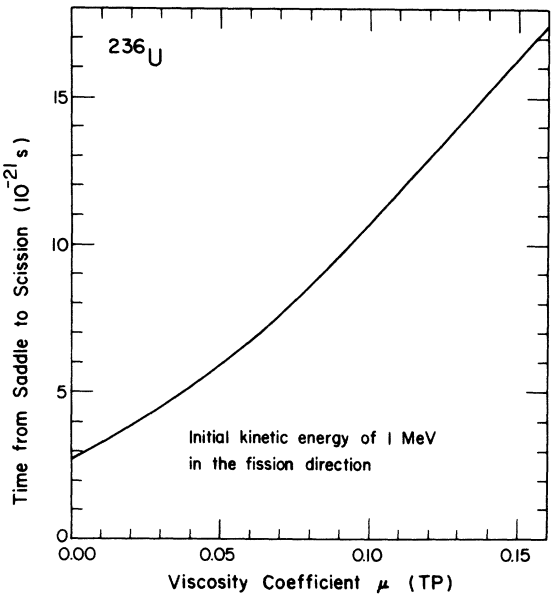

FIG. 2. Time required for a ^{236}U nucleus to travel from its macroscopic saddle point to scission, as a function of the two-body viscosity coefficient μ. The initial conditions correspond to starting from the saddle point with 1 MeV of kinetic energy in the fission direction.

finitesimal distance from the saddle point are indistinguishable on the scale of this figure. An increase in the value of σ for a fixed value of r corresponds to an increase in the neck radius. This figure clearly shows the viscosity-induced inhibition of neck formation mentioned above.

Figure 3 illustrates another important point that is relevant to the statistical theory of fission.[53] Attempts have been made to justify this

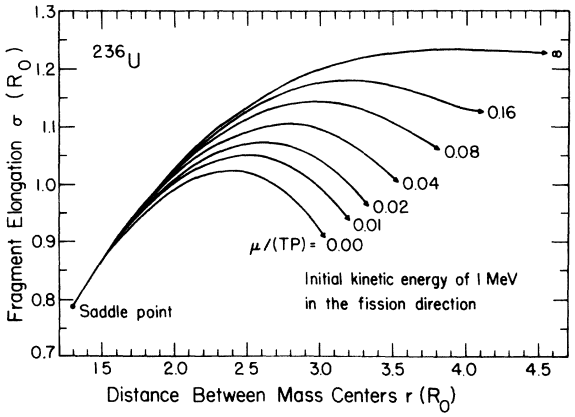

FIG. 3. Dynamical paths in r-σ space of a ^{236}U nucleus from its macroscopic saddle point to scission, for various values of the two-body viscosity coefficient μ. The scission points are indicated by the tips of the arrowheads.

theory on the grounds that nuclei are very viscous and therefore will follow the path of steepest descent in the potential-energy surface.[53] It is well known that for nonviscous nuclei the dependence upon shape of the inertia tensor causes the dynamical fission path to deviate from the path of steepest descent.[54] It is less well known but equally true that the viscosity tensor has a similar effect. In fact, the path of steepest descent in Fig. 3 lies below the $\mu = 0$ path, and increasing the two-body viscosity increases rather than decreases the deviations from this path. A nucleus with large two-body viscosity therefore follows a path that is even farther away from the path of steepest descent than does a nonviscous nucleus, which means that this justification for the statistical theory of fission is invalid.

In Fig. 4 we illustrate the effect of viscosity on the postscission motion of the fission fragments. As discussed in Sec. IID, the fission fragments are described in terms of two separated spheroids. The postscission motion consists of a separation of the centers of mass of the two fragments, coupled with motion of the fragments about their own centers of mass. Configu-

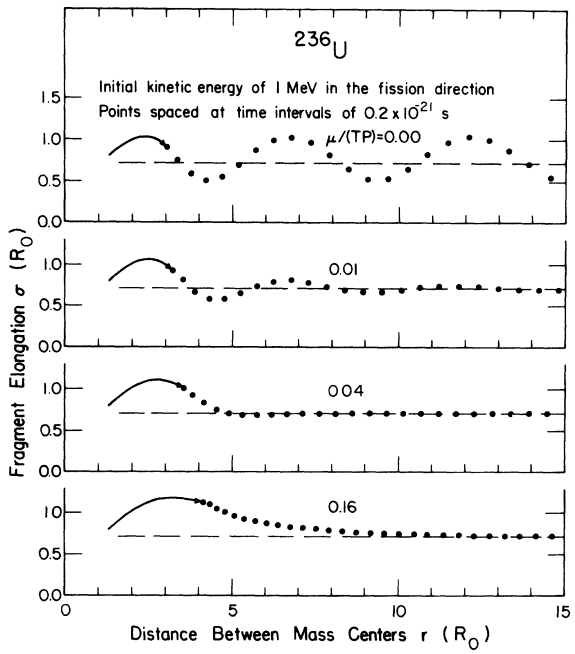

FIG. 4. Dynamical paths in r-σ space of a ^{236}U nucleus, for various values of the two-body viscosity coefficient μ. The paths from the macroscopic saddle point to scission are given by the solid curves. The postscission paths of the fission fragments are given by the solid circles, which are equally spaced in time at intervals of 0.2×10^{-21} s. The thin horizontal long-dashed lines denote configurations of two separated spherical nuclei.

rations of two separated spherical nuclei are indicated in the figure by the thin horizontal long-dashed lines.

For zero viscosity the fragments oscillate about their centers all the way to infinity, at which point the excitation energy is entirely in the form of collective vibrational energy. For finite values of viscosity, the energy of collective motion is dissipated during the separation, and the excitation energy at infinity is entirely in the form of internal energy. When the viscosity is small, the fragments still oscillate but with amplitudes that decrease as they separate. Above a critical viscosity, whose value is roughly 0.1 TP, the fragments no longer oscillate but instead their elongation decreases nearly exponentially as they separate.

For small values of viscosity a portion of the total interaction energy at scission is converted into fragment vibrational kinetic energy rather than into translational kinetic energy. This can be seen in Fig. 4 for zero viscosity by the increase in the maximum fragment elongation σ after one complete oscillation relative to the fragment elongation at scission. For infinite viscosity, the fragments retain their shape as they separate, and the total interaction energy at scission is converted entirely into translational kinetic energy.

B. Spontaneous fission of ^{252}Cf

As another example, we consider the motion of a ^{252}Cf nucleus after it has penetrated the fission barrier in spontaneous fission. For this purpose we start the system at rest from the point that it emerges after penetrating the macroscopic fission barrier at zero potential energy. The barrier is calculated for the fission coordinate y that is defined in terms of liquid-drop-model saddle-point shapes.[10,55] The nuclear macroscopic energy is again calculated in terms of a double volume integral of a Yukawa function.

Figure 5 illustrates how two-body viscosity decreases the translational kinetic energy that is acquired for a given separation of the centers of mass. The vertical arrows denote the zero-neck-radius scission configuration, which becomes more elongated with increasing viscosity. For zero viscosity the centers of mass at scission are separated by 23.7 fm and the translational kinetic energy is 58 MeV, whereas for $\mu = 0.08$ TP the corresponding values are 30.2 fm and 27 MeV.

Our initial hope was that we could determine the viscosity coefficient by comparing the results of Fig. 5 with scission-point properties deduced from analyses of light particles emitted during the spontaneous fission of ^{252}Cf. However, this does not appear to be possible because of the different dynamical path taken for fission accompanied by the emission of light particles relative to the path taken in normal fission (where no light particles are emitted).[56]

In Fig. 6 we show the dependence of the neck radius upon the distance between mass centers, for dynamical paths calculated with various amounts of two-body viscosity. This figure illustrates once again that two-body viscosity hinders neck formation and leads to a more elongated scission configuration.

Both because of the more elongated scission con-

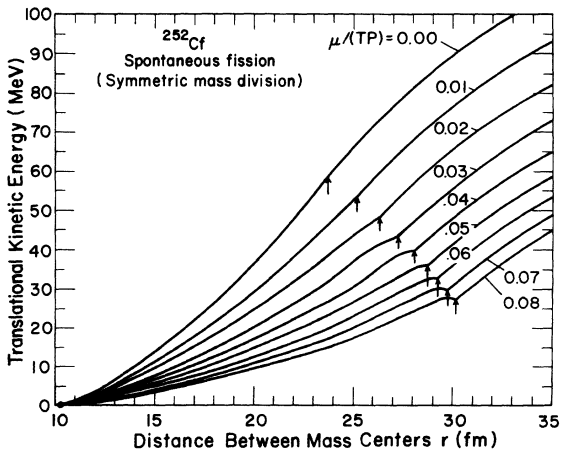

FIG. 5. Dependence of the translational kinetic energy acquired during the symmetric spontaneous fission of ^{252}Cf upon the distance between mass centers r, for various values of the two-body viscosity coefficient μ. The scission points are indicated by the vertical arrows.

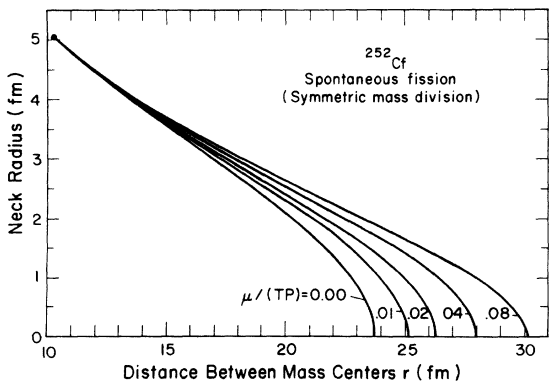

FIG. 6. Dependence of the neck radius in the symmetric spontaneous fission of ^{252}Cf upon the distance between mass centers r, for dynamical paths calculated with various values of the two-body viscosity coefficient μ.

figuration and because of the smaller translational kinetic energy at scission, the final translational kinetic energy at infinity decreases with increasing two-body viscosity. This is illustrated by the bottom curve in Fig. 7.

We also show in Fig. 7 the effect on the final kinetic energy of the neck rupturing before its radius reaches zero. Where this is expected to occur in the fission of an actual nucleus may be estimated by determining the area of the neck that is required for the attractive nuclear force to withstand the repulsive Coulomb force. In making this estimate, we approximate the nuclear force per unit area in terms of a Yukawa interaction[40] between two semi-infinite slabs of nuclear matter. The Coulomb force is approximated by the force between two equal spheres separated by 21.5 fm, which is a nominal value deduced from an analysis[56] of the light particles accompanying the spontaneous fission of ^{252}Cf. This yields a neck radius of about 1.2 fm at which rupture should occur.

In calculating the effect of a finite scission neck radius upon the fission-fragment translational kinetic energy at infinity, the postscission motion of the fission fragments is again described in terms of separated spheroids. The initial conditions for the postscission motion are determined by making continuous the values of r, σ, $\dot{r}$, and $\dot{\sigma}$ at the scission point (which now occurs at a finite neck radius). As seen in Fig. 7, the calculated kinetic energy at infinity increases slightly as the scission neck radius increases. As indicated by the dashed line in Fig. 7, the kinetic energy also increases when scission is assumed to occur at a constant distance between mass centers of 21.5 fm.

The shaded band in Fig. 7 gives the experimental value of the average fission-fragment kinetic energy corresponding to a symmetric mass division for ^{252}Cf spontaneous fission.[57] The experimental value is reproduced by the calculations for a two-body viscosity coefficient μ of 0.007 TP when the scission neck radius is taken to be zero. The viscosity coefficient increases to 0.009 TP for a scission neck radius of 1.2 fm, and to 0.017 TP for a scission neck radius of 2.0 fm or a distance between mass centers at scission of 21.5 fm. However, because in the spontaneous fission of ^{252}Cf the kinetic energy is affected strongly by single-particle corrections, we do not place significant weight upon this comparison. We return in Sec. III D to a determination of the viscosity coefficient from a comparison with experimental kinetic energies at high excitation energies, where single-particle corrections are much less important. Because of the relatively small effect of a 1.2-fm scission neck radius on the final translational kinetic energy, the scission neck radius is taken to be zero throughout the remainder of the paper.

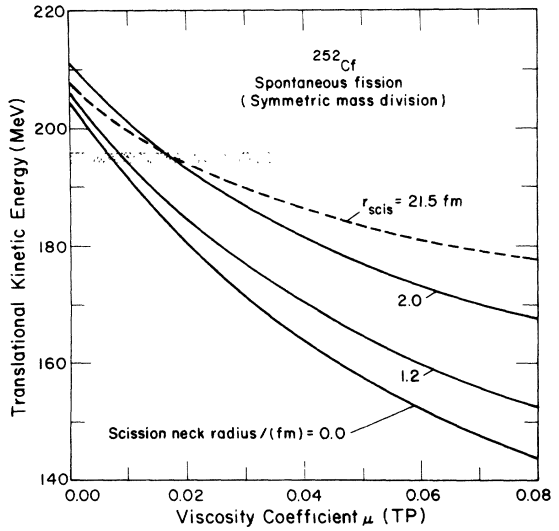

FIG. 7. Fission-fragment translational kinetic energies at infinity for the symmetric spontaneous fission of ^{252}Cf, as functions of the two-body viscosity coefficient μ. For the three solid curves the neck is assumed to rupture at the indicated value of the neck radius, whereas for the dashed curve the neck is assumed to rupture when the nascent-fragment mass centers are separated by 21.5 fm. The experimental most probable kinetic energy for equal mass division (Ref. 57) is given by the shaded band.

C. Fission of nuclei throughout the Periodic Table

We turn now to the effect of two-body viscosity on the fission of nuclear systems throughout the Periodic Table. For this purpose we use the pure liquid-drop model, in which the nuclear system is characterized by the fissility parameter

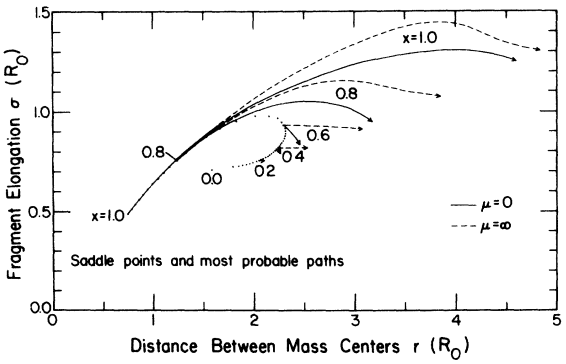

FIG. 8. Liquid-drop-model saddle points (solid circles) and most probable dynamical paths for various values of the fissility parameter x. The paths for zero viscosity are given by solid curves, and those for infinite viscosity are given by dashed curves. The scission points are indicated by the tips of the arrowheads.

x defined by Eq. (9). The nuclear potential energy is measured in units of the spherical surface energy $E_s^{(0)}$ defined by Eq. (7), and the two-body viscosity coefficient is measured in the natural unit[19]

$$\mu_0 = [M_0 E_s^{(0)}]^{1/2}/R_0^2 \ . \tag{22}$$

For a heavy nucleus the value of μ_0 is roughly 1 TP.

In the fission of heavy nuclei, where the saddle-point shapes are cylinder-like, the distance from the saddle point to scission is much longer than in the fission of light nuclei, where the saddle-point shapes are dumbbell-like.[14,17,18,58] In this context the transition between heavy and light nuclei occurs at $x \approx 0.67$, which corresponds roughly to radium. This difference is illustrated in Fig. 8, where for five values of the fissility parameter we show the most probable dynamical paths for zero viscosity (solid curves) and infinite two-body viscosity (dashed curves). Near $x = 1$ the most probable paths follow closely the sequence of liquid-drop-model saddle-point shapes (indicated by the solid points). This demonstrates that the frequently used fission coordinate y[10,55] is adequate for small deformations, but beyond $y \approx 0.3$ the most probable path diverges from the sequence of liquid-drop-model saddle-point shapes.

The initial most probable fission direction (the fission eigenvector) is in general determined by the stiffness, inertia, and viscosity tensors at the saddle point. For zero viscosity this direction is determined by the stiffness and inertia tensors alone, whereas for infinite viscosity it is determined by the stiffness and viscosity tensors alone. As $x \to 1$ all three tensors become diagonal in terms of second-order Legendre-polynomial distortions, so that the initial directions for zero viscosity and infinite viscosity coincide. However, for light nuclei the initial direction corresponds primarily to a contraction of the neck for small viscosity, and primarily to a separation of mass centers for large two-body viscosity.

As the two-body viscosity coefficient increases, the dynamical path in general shifts monotonically away from the nonviscous path in the direction of increased fragment elongation, and the scission configuration is more elongated. However, for values of x close to 1 the dynamical path near the scission point for infinite two-body viscosity lies somewhat below those for large finite values of viscosity, and the scission configuration is somewhat less elongated. This crossover in the dynamical paths is caused by an inertial effect for finite viscosity.

In Fig. 9 we see the effect of two-body viscosity on both the prescission translational kinetic energy (dashed curves) and the total translational kinetic energy at infinity (solid curves). Because of the transition at $x \approx 0.67$ in saddle-point properties, the results are qualitatively different for heavy nuclei and for light nuclei. For heavy nuclei, increasing the viscosity reduces the prescission kinetic energy, which in the absence of viscosity is considerable because of the relatively long distance from the saddle point to scission. For light nuclei the short distance from the saddle point to scission means that the prescission kinetic energy is small for all values of viscosity. However, because the effect of two-body viscosity is to increase the distance from saddle to scission, a viscous system has a longer distance in which to acquire prescission kinetic energy than does a nonviscous one. Because of this, the prescission kinetic energy for light nuclei increases slightly

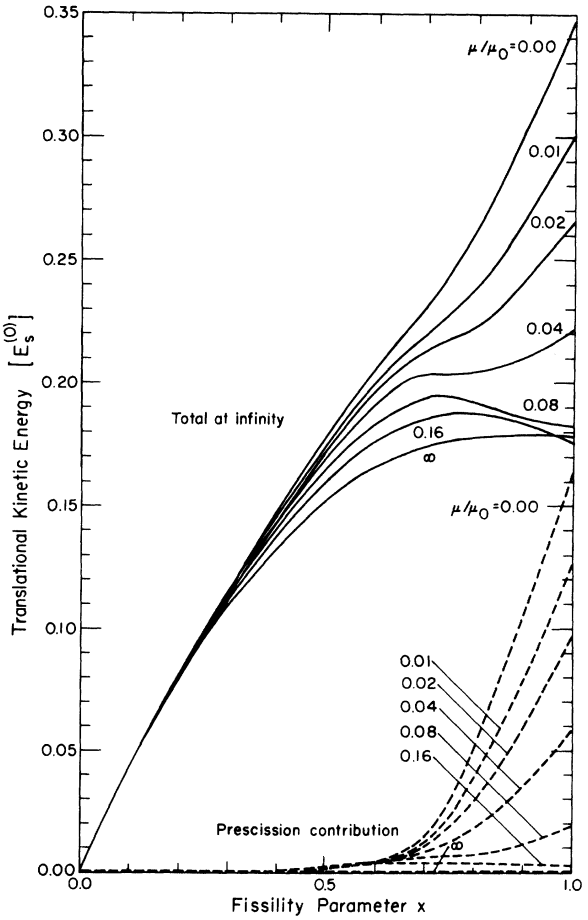

FIG. 9. Dependence of the fission-fragment translational kinetic energy upon the fissility parameter x, for various values of the two-body viscosity coefficient μ. The natural unit of viscosity μ_0 is given by Eq. (22). The dashed curves give the translational kinetic energy acquired prior to scission, and the solid curves give the value at infinity.

for small values of viscosity, although it is of course zero for infinite viscosity.

The translational kinetic energy at infinity is the sum of the prescission translational kinetic energy and the translational kinetic energy acquired after scission. In the liquid-drop model the latter arises primarily from the Coulomb interaction energy at scission, although it is not given exactly by this quantity because in general some of the interaction energy is converted into vibrational energy and subsequently into internal excitation energy rather than into translational kinetic energy.

For heavy nuclei the translational kinetic energy at infinity in general decreases with increasing two-body viscosity both because the prescission contribution is less and because the Coulomb interaction energy at scission is less. That fraction of the Coulomb interaction energy that goes into translational kinetic energy decreases for small values of viscosity because of the increased time the fission fragments spend with significant oblate deformations during their separation relative to the time with prolate shapes.[19] For large viscosity the fraction increases because the fission fragments remain prolate for a significantly longer time during the initial separation stage.

For values of x close to 1 the total translational kinetic energy for large finite viscosity is smaller than that for infinite viscosity because of the crossover in the dynamical paths discussed earlier. For light nuclei the total translational kinetic energy depends very little upon viscosity, as a result of the short distance from the saddle point to scission.

The energy released in going from the saddle point to infinite separation of the fission fragments is divided into translational kinetic energy, which we have just considered, plus excitation energy. As shown in Fig. 10, the excitation energy increases with increasing fissility parameter x, and also in general increases with increasing two-body viscosity. However, for values of x close to 1, the crossover in the dynamical paths discussed earlier leads to a slightly smaller excitation energy for infinite viscosity than for large finite viscosity. At infinite fission-fragment separation the excitation energy remains entirely in the form of collective energy for zero viscosity, but is entirely converted into internal energy for all finite values of viscos-

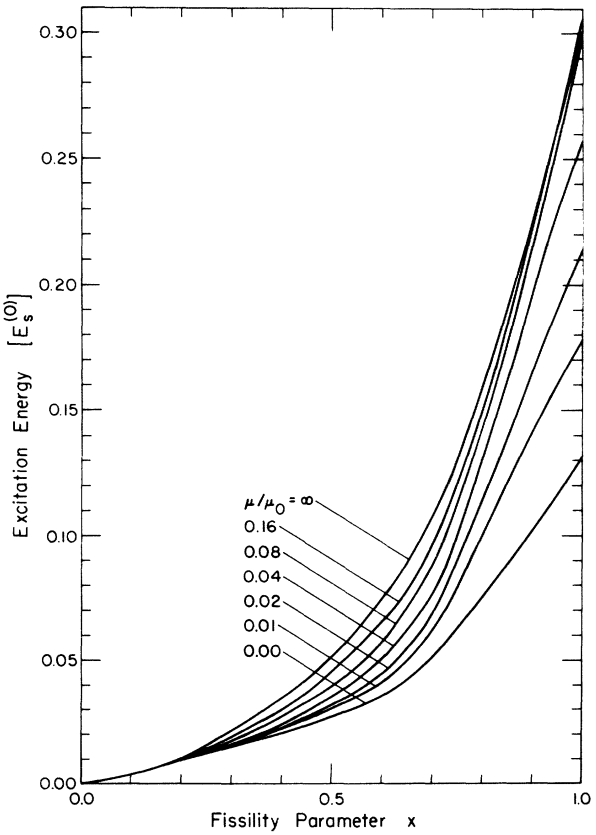

FIG. 10. Dependence of the fission-fragment excitation energy at infinity upon the fissility parameter x, for various values of the two-body viscosity coefficient μ. The natural unit of viscosity μ_0 is given by Eq. (22).

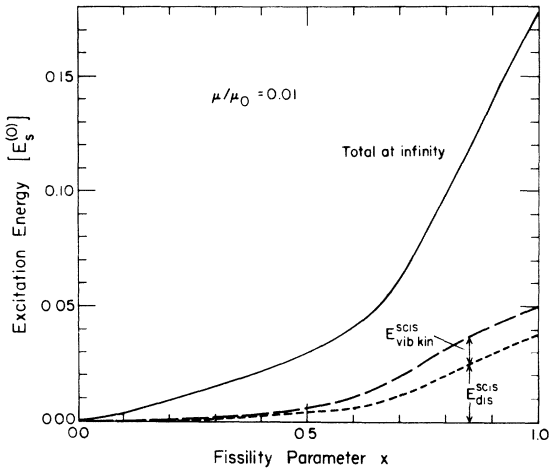

FIG. 11. Decomposition of the fission-fragment excitation energy into its various components at scission, as a function of the fissility parameter x. The two-body viscosity coefficient μ has the value $0.01\mu_0$, where the natural unit of viscosity μ_0 is given by Eq. (22). The dashed curve gives the energy dissipated into internal energy prior to scission, and the difference between the long-dashed curve and the short-dashed curve gives the vibrational kinetic energy at scission. The remaining energy, given by the difference between the solid curve and the long-dashed curve, is in the form of potential energy at scission.

ity.

The energy that appears ultimately as excitation energy is in several different forms at the scission point, as illustrated in Fig. 11 for $\mu = 0.01\mu_0$. The short-dashed curve gives the dissipated energy $E_{\rm dis}^{\rm scis}$ that is in the form of internal energy already at the scission point; this quantity in general increases with increasing viscosity. The difference between the long-dashed curve and the short-dashed curve represents the vibrational kinetic energy $E_{\rm vib\,kin}^{\rm scis}$ at the scission point; an increase in viscosity in general decreases this quantity. The remaining energy, which is given by the difference between the solid curve and the long-dashed curve, is primarily potential energy of deformation at scission, but also contains that portion of the Coulomb interaction energy at scission that is converted during the dynamical postscission motion into vibrational energy and ultimately into internal excitation energy rather than into translational kinetic energy. This remaining energy also in general increases with increasing viscosity.

D. Comparison with experimental fission-fragment kinetic energies

We have considered up to this point the effect on the dynamics of fission of varying the two-body viscosity coefficient μ from 0 to ∞. Provided that nuclear dissipation proceeds primarily by means of two-body collisions, we now proceed to determine the average value of μ at high excitation energies by comparing calculated and experimental most probable fission-fragment kinetic energies for the fission of nuclei throughout the Periodic Table. However, we should stress from the outset that this comparison does not imply that nuclear dissipation is necessarily of the two-body type.

In making this comparison, which is shown in Fig. 12, we take into account the finite range of the nuclear force when calculating the nuclear macroscopic energy. This is done both because this effect is present in the fission of real nuclei and because the available constants for the finite-range model[40] are more appropriate for calculating fission-fragment kinetic energies than are the best available constants for the liquid-drop model.[46] In particular, the value of 1.16 fm that is used here for the nuclear-radius constant r_0 describes adequately the average equivalent-sharp spatial extent of nuclei throughout the Periodic Table.[47,48] (The value of 1.18 fm given in Ref. 48 refers to infinite nuclear matter. The squeezing of finite nuclei by the surface tension and their dilation by the Coulomb repulsion lead to an effective value which varies slightly throughout the Periodic Table but which is 1.16 fm for medium-weight nuclei.)

By comparison, the frequently used value of 1.2249 fm in the liquid-drop model[46] gives nuclei that are about 6% too large and consequently fission-fragment kinetic energies that are about 6% lower than values calculated with the correct nuclear-radius constant. It is primarily the use of the larger value of 1.2249 fm for the nuclear-radius constant that explains why in Ref. 17 the experimental kinetic energies lie above the calculated

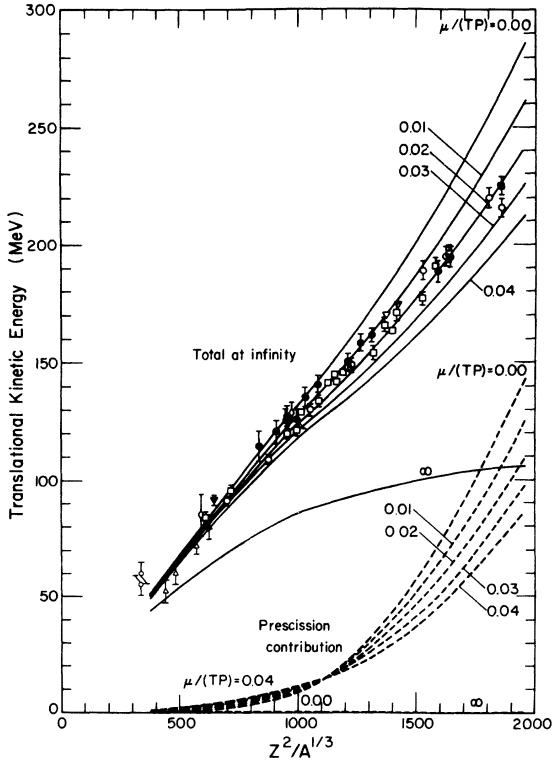

FIG. 12. Comparison of experimental most probable fission-fragment kinetic energies with results calculated for different values of the viscosity coefficient μ (solid curves). The calculations include the effect of the finite range of the nuclear force on the nuclear macroscopic energy. The experimental data are for the fission of nuclei at high excitation energies, where the most probable mass division is into two equal fragments. The open symbols represent values for equal mass divisions only, and the solid symbols represent values averaged over all mass divisions. Open circles are used for data obtained in Ref. 60, and open squares are used for data obtained in Refs. 61–64 and reported in Ref. 60. Open downward-pointing triangles refer to Ref. 65, open upward-pointing triangles to Ref. 66, open diamonds to Ref. 67, and open hexagons to Ref. 68. Solid circles are used for data obtained in Ref. 69 and corrected in Ref. 70. The solid square refers to Ref. 71 and the solid downward-pointing triangle to Ref. 72. The dashed curves give the calculated translational kinetic energies acquired prior to scission.

curve for zero viscosity. However, two other differences are the use in Ref. 17 of the liquid-drop model and a simpler approximation for the post-scission motion than is used here.

When the finite range of the nuclear force is taken into account, it is no longer strictly possible to display the results calculated for all nuclei as functions of a single parameter. We therefore adopt the expedient of calculating the results for nuclei along Green's approximation to the valley of β stability;[59] the calculated kinetic energies are then plotted in units of MeV as functions of $Z^2/A^{1/3}$ for the nuclear system undergoing fission. The accuracy of this procedure turns out to be excellent, as verified by performing additional calculations for the actual nuclear system $^{278}110$, which is moderately far removed from the valley of β stability.

The transition from cylinder-like saddle-point shapes for heavy nuclei to dumbbell-like saddle-point shapes for light nuclei is more gradual in the finite-range model[40] than in the liquid-drop model.[14,17,18,58] Because of this, the transition that occurs in Fig. 12 at $Z^2/A^{1/3} \approx 1100$ is more gradual than the analogous transition that occurs in Fig. 9 at $x \approx 0.67$.

Experimental most probable fission-fragment kinetic energies[60-72] for the fission of nuclear systems ranging from ^{80}Sr to $^{278}110$ are included in Fig. 12. These data all refer to moderately high excitation energies, where the most probable mass division is into two equal fragments and where single-particle effects on the nuclear potential energy of deformation should be reduced. Open symbols represent values for equal mass divisions only, and solid symbols represent values averaged over all mass divisions. (The opposite convention concerning open and solid symbols stated in Ref. 21 is erroneous.)

Some of the experimental kinetic energies in Fig. 12 are strictly "most probable" values, whereas the remainder are in fact average values; in accordance with usual practice we use most probable to refer loosely to both types of data. All experimental data in the figure have been corrected for the effects of neutron emission from the fragments and for calibration effects. No corrections have been made for angular-momentum effects, which are possibly large for those data that refer to fission induced by very heavy ions.

It is seen from Fig. 12 that the value

$$\mu = 0.015 \pm 0.005 \text{ TP} = 9 \pm 3 \times 10^{-24} \text{ MeV s/fm}^3$$

accounts for most of the experimental data to within their uncertainties, although there is a clear variation in the optimum value of μ from about 0.01 TP for the lighter systems to about 0.02 TP for the heavier systems. By coincidence, 0.015 TP is the same value obtained earlier by Wieczorek, Hasse, and Süssman[37-39] by integrating the Rayleigh dissipation function along the nonviscous ^{236}U path from saddle to scission and by assuming arbitrarily that 10 MeV of energy is dissipated along this path.

The deduced value of μ may be compared with the value that is required to critically damp the quadrupole oscillations of idealized nuclei, which is approximately 0.05 TP for heavy actinide nuclei and approximately 0.08 TP for medium-weight nuclei. (In Ref. 20 it is implied erroneously that the critical viscosity coefficient for idealized heavy nuclei is about 0.1 TP.)

IV. SUMMARY AND CONCLUSION

In this study of the dynamics of large-scale nuclear shape changes we have used a simple macroscopic approach in which the nuclear shape is parametrized in terms of a few relevant degrees of freedom. The dissipation of energy from collective motion into internal single-particle motion was calculated under the assumption that nuclear dissipation arises from two-body collisions. We have studied the time evolution of fissioning nuclei by solving numerically the classical equations of motion with appropriate initial conditions.

In addition to slowing down the dynamical descent of a fissioning nucleus from its saddle point, two-body viscosity hinders the formation of a neck, which leads to a more elongated scission configuration. Because of both the slowing down and the increased scission elongations, the calculated fission-fragment translational kinetic energy decreases with increasing two-body viscosity.

This permitted us to determine the average value of the two-body viscosity coefficient that reproduces experimental most probable fission-fragment kinetic energies for the fission at high excitation energies of nuclei throughout the periodic table. The result is

$$\mu = 0.015 \pm 0.005 \text{ TP} = 9 \pm 3 \times 10^{-24} \text{ MeV s/fm}^3 ,$$

which is about 30% of the value that is required to critically damp the quadrupole oscillations of idealized heavy actinide nuclei. Thus, provided that nuclear dissipation arises primarily from two-body collisions, nuclei are only moderately viscous.

However, because of the relatively long mean free path of nucleons inside a nucleus, it is entirely possible that nuclear dissipation arises primarily from nucleons colliding with the moving boundary of the nucleus rather than with each other.[32-35] This one-body dissipation has proper-

ties that are qualitatively opposite[34,35] those for the two-body viscosity considered here. In particular, one-body dissipation enhances the formation of a neck, which leads to a more compact scission configuration. Fission-fragment kinetic energies calculated on the basis of one-body dissipation[35] agree with the experimental values equally well as do our present calculations with two-body viscosity.

The basic mechanism of nuclear dissipation—whether by means of individual nucleon collisions with each other or by means of nucleon collisions with the moving boundary of the nucleus—is therefore still open. In deciding this important question we hope that the results presented here for the former mechanism will prove useful.

We are grateful to J. Péter for his assistance with collecting the experimental data used in Fig. 12, and to W. J. Swiatecki for stimulating discussions concerning one-body dissipation.

APPENDIX A: DERIVATION OF THE INERTIA AND VISCOSITY TENSORS

By virtue of the equation of continuity the velocity field $\vec{v}$ for an incompressible fluid satisfies

$$\nabla \cdot \vec{v} = 0. \tag{A1}$$

The total kinetic energy of the system is given by

$$T = \tfrac{1}{2}\rho_m \int v^2 d^3r \ , \tag{A2}$$

where

$$\rho_m = M_0/(\tfrac{4}{3}\pi R_0^3) \tag{A3}$$

is the constant mass density and where the integration is over the volume of the shape.

In order to express T in the form of Eq. (12), it is necessary that the position vector $\vec{r}$ of a fluid element not involve the time *explicitly*; instead, it must depend only upon the shape of the system.[73] This permits us to write

$$\vec{v} = \dot{\vec{r}}(q) = \sum_i \frac{\partial \vec{r}}{\partial q_i}\dot{q}_i \ , \tag{A4}$$

which, upon substituting into Eq. (A2) and performing the volume integration, expresses T in the form of Eq. (12).

We specialize to axially symmetric shapes, for which the velocity is given in cylindrical coordinates by

$$\vec{v} = \dot{\rho}\hat{e}_\rho + \dot{z}\hat{e}_z \ , \tag{A5}$$

where $\hat{e}_\rho$ and $\hat{e}_z$ denote unit vectors in the ρ and z directions, respectively. The Werner-Wheeler method[17,23,42] is equivalent to assuming that $\dot{z}$ is independent of ρ and that $\dot{\rho}$ depends linearly upon ρ, i.e.,

$$\dot{z} = \mathcal{A}(z;q,\dot{q}) = \sum_i A_i(z;q)\dot{q}_i \tag{A6a}$$

and

$$\dot{\rho} = \rho\mathcal{B}(z;q,\dot{q}) = \frac{\rho}{P}\sum_i B_i(z;q)\dot{q}_i \ , \tag{A6b}$$

where $P = P(z;q)$ is the value of ρ on the surface of the shape at the position z.

In previous studies of the Werner-Wheeler method, which were restricted to nonviscous flow, the expansion coefficients B_i were related to the coefficients A_i by use of the kinematical boundary condition on the system's surface. We find it more convenient here, where we must calculate the viscosity tensor in addition to the inertia tensor, to use instead the interior relation (A1) to obtain

$$\mathcal{B} = -\frac{1}{2}\frac{\partial \mathcal{A}}{\partial z} \tag{A7}$$

or

$$B_i = -\frac{1}{2}P\frac{\partial A_i}{\partial z} \ . \tag{A8}$$

Upon substituting Eqs. (A5), (A6), and (A8) into Eq. (A2) and comparing with Eq. (12), we obtain for the elements of the inertia tensor the result

$$M_{ij} = \pi\rho_m \int_{z_{\min}}^{z_{\max}} P^2(A_iA_j + \tfrac{1}{8}P^2A_i'A_j')dz \ , \tag{A9}$$

where the primes denote differentiation with respect to z.

The expansion coefficients A_i are determined from the condition that for an incompressible fluid the total (convective) time derivative of any fluid volume must vanish.[74] We denote by

$$V^+(z;q) = \pi\int_z^{z_{\max}} P^2(z';q)dz' \tag{A10a}$$

and

$$V^-(z;q) = \pi\int_{z_{\min}}^{z} P^2(z';q)dz' \tag{A10b}$$

the volumes of the fluid to the right and to the left, respectively, of a plane perpendicular to the symmetry axis at the point z. It then follows that

$$\begin{aligned}\frac{d}{dt}V^+(z;q) &= \frac{\partial V^+}{\partial z}\dot{z} + \sum_i \frac{\partial V^+}{\partial q_i}\dot{q}_i \\ &= \pi\left\{-P^2(z;q)\dot{z} + \sum_i\left[\frac{\partial}{\partial q_i}\int_z^{z_{\max}} P^2(z';q)dz'\right]\dot{q}_i\right\} \\ &= 0 \ ,\end{aligned} \tag{A11}$$

or

$$\dot{z} = \frac{1}{P^2(z;q)} \sum_i \left[\frac{\partial}{\partial q_i} \int_z^{z_{\max}} P^2(z';q)dz' \right] \dot{q}_i \ . \quad \text{(A12)}$$

Upon comparing Eqs. (A6a) and (A12), we see that[17]

$$A_i(z;q) = \frac{1}{P^2(z;q)} \frac{\partial}{\partial q_i} \int_z^{z_{\max}} P^2(z';q)dz' \ , \quad \text{(A13a)}$$

which is an expression that is especially useful for calculating A_i for values of z to the right of the body's midplane. Also, we obtain in a similar way, by taking the total time derivative of $V(z;q)$, the alternative formula[17]

$$A_i(z;q) = -\frac{1}{P^2(z;q)} \frac{\partial}{\partial q_i} \int_{z_{\min}}^{z} P^2(z';q)dz' \ , \quad \text{(A13b)}$$

which is especially useful for calculating A_i for values of z to the left of the midplane.

For an incompressible fluid with a constant two-body viscosity coefficient μ, the Rayleigh dissipation function is given by[75]

$$F = \tfrac{1}{2}\mu \int \Phi(\vec{r})d^3\gamma \ , \quad \text{(A14)}$$

where

$$\Phi(\vec{r}) = \nabla^2 v^2 + \omega^2 - 2\nabla \cdot (\vec{v} \times \vec{\omega}) \quad \text{(A15)}$$

and where

$$\vec{\omega} = \nabla \times \vec{v} \quad \text{(A16)}$$

is the vorticity.

Insertion of Eqs. (A5) and (A6) into this result leads to

$$\Phi = 4\mathfrak{B}^2 + \rho^2(\mathfrak{B}')^2 + 4\mathfrak{A}\mathfrak{B}' + 2[(\mathfrak{A}')^2 + \mathfrak{A}\mathfrak{A}''] \ , \quad \text{(A17)}$$

where the single and double primes denote, respectively, first and second derivatives with respect to z. By virtue of Eq. (A7) this simplifies further to

$$\Phi = 3(\mathfrak{A}')^2 + \tfrac{1}{4}\rho^2(\mathfrak{A}'')^2 \ . \quad \text{(A18)}$$

Upon substituting Eqs. (A6a) and (A18) into Eq. (A14) and comparing with Eq. (13) we obtain for the elements of the viscosity tensor the result

$$\eta_{ij} = \pi\mu \int_{z_{\min}}^{z_{\max}} P^2(3A_i'A_j' + \tfrac{1}{5}P^2A_i''A_j'')dz \ . \quad \text{(A19)}$$

APPENDIX B: ACCURACY OF THE WERNER-WHEELER METHOD

As an approximation to incompressible, nonviscous irrotational flow, the Werner-Wheeler method is known to be excellent for shapes involved in the early stages of fission.[17] Here we study the accuracy of this method as an approximation to incompressible *viscous* flow.

As the viscosity increases from zero, the exact hydrodynamical flow deviates from irrotational flow. This causes the exact hydrodynamical inertia to increase, as required by Kelvin's theorem that the kinetic energy for irrotational flow is a minimum.[76] The viscosity tensor is proportional to the viscosity coefficient μ. However, the proportionality factor depends upon the hydrodynamical flow and therefore upon the viscosity.

Because the Navier-Stokes equations for incompressible viscous flow are harder to solve than the Euler equations for nonviscous flow, it is more difficult in the presence of viscosity to determine the accuracy of the inertia and viscosity tensors calculated by use of the Werner-Wheeler method. However, exact solutions are available for the small motions about a spherical equilibrium shape of a viscous fluid under the influence of gravitational (or electrostatic) forces and/or surface tension.[9,77-81]

The normal modes of a viscous sphere have spherical-harmonic angular behavior, with an infinite number of radial eigenfunctions for each order of spherical harmonic. The normal modes have the time dependence $\exp(-\sigma_{nk}t)$, where n labels the degree of the spherical harmonic and where k is the index of the radial eigenfunction. For a given degree n, the two lowest values of σ_{nk} are either both real and positive or complex conjugates, depending upon whether the system is overdamped or underdamped; the other roots are all positive and real. Some numerical values of the roots are given in Refs. 78, 80, and 81.

Upon restricting the discussion to axially symmetric motions and working to first order in the coordinates and momenta, we may expand the system's radius vector in a series of Legendre polynomials,

$$R = R_0 \left[1 + \sum_{n=1}^{\infty} \alpha_n P_n(\cos\theta) \right],$$

where R_0 is the radius of the spherical shape. Evaluation of Eqs. (A2)–(A5) and (A14)–(A16) for hydrodynamical flow in the limit of zero viscosity (irrotational flow) then yields for the diagonal elements of the inertia[82] and viscosity[36,81] tensors

$$M_n^{\text{irr}} = \frac{3}{n(2n+1)} M_0 R_0^2$$

and

$$\eta_n^{\text{irr}} = 8\pi \frac{(n-1)}{n} R_0^3 \mu \ ,$$

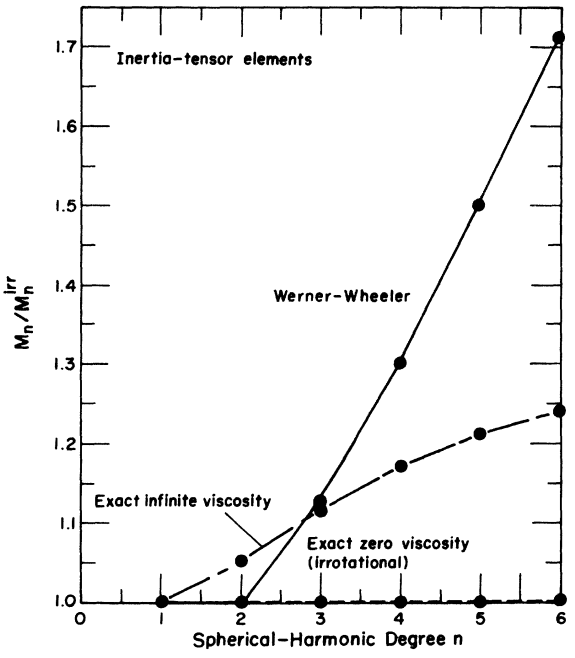

FIG. 13. Comparison of the diagonal elements M_n of the inertia tensor for three types of hydrodynamical flow about a spherical shape. The solid curve gives the result for Werner-Wheeler flow, the short-dashed curve gives the result for nonviscous irrotational flow, and the dot-dashed curve gives the result for infinitely viscous flow. The quantity that is actually plotted is the inertia for a particular type of flow divided by the inertia for irrotational flow.

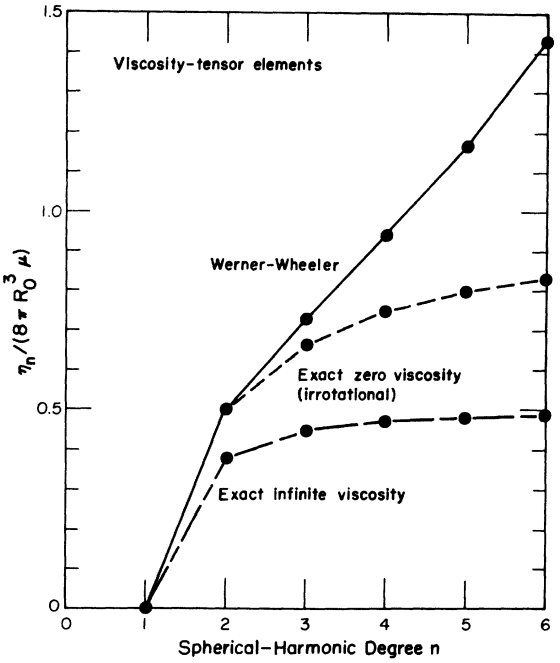

FIG. 14. Comparison of the diagonal elements η_n of the two-body viscosity tensor for three types of hydrodynamical flow about a spherical shape. The solid curve gives the result for Werner-Wheeler flow, the short-dashed curve gives the result in the limit of nonviscous irrotational flow, and the dot-dashed curve gives the result in the limit of infinitely viscous flow. The results are plotted in units of $8\pi R_0^3\mu$, where R_0 is the radius of the sphere and where μ is the two-body viscosity coefficient.

where M_0 is the total mass of the system and where μ is the two-body viscosity coefficient.

Evaluation of the same equations for hydrodynamical flow corresponding to the lowest radial eigenfunction in the limit of infinite two-body viscosity yields[81,83]

$$M_n^{\infty}=\left[1+\frac{4(n+1)(n-1)^2}{(2n+1)^2(2n+5)}\right]M_n^{\mathrm{irr}}$$

and[84]

$$\eta_n^{\infty}=\left[\frac{2(n+1)^2+1}{(2n+1)^2}\right]\eta_n^{\mathrm{irr}}\ .$$

In the Werner-Wheeler method, the velocity field corresponding to a given Legendre-polynomial distortion n is

$$\vec{v}_n=-\left[\frac{\rho P_n^2(\cos\theta)}{n(n+1)\sin^4\theta}\,\hat{e}_\rho+\frac{2R_0P_n^1(\cos\theta)}{n(n+1)\sin^2\theta}\,\hat{e}_z\right]\dot{\alpha}_n$$

and the corresponding curl is

$$\nabla\times\vec{v}_n=\frac{\rho P_n^3(\cos\theta)}{n(n+1)\sin^3\theta R_0}\,\hat{e}_\phi\dot{\alpha}_n\ ,$$

where $\hat{e}_\rho$, $\hat{e}_z$, and $\hat{e}_\phi$ are cylindrical-coordinate unit vectors in the ρ, z, and ϕ directions, respectively, and where P_n^m is an associated Legendre polynomial of degree n and order m.[85] Evaluation of Eqs. (A2)–(A5) and (A14)–(A16) with this Werner-Wheeler flow then yields

$$M_n^{\mathrm{WW}}=\left[\frac{n^2+n+6}{4(n+1)}\right]M_n^{\mathrm{irr}}$$

and

$$\eta_n^{\mathrm{WW}}=\left[\frac{(n+2)(n^2+n+30)}{48(n+1)}\right]\eta_n^{\mathrm{irr}}\ .$$

In Fig. 13 we compare the six lowest elements of the inertia tensor calculated by use of the Werner-Wheeler method with the results for zero viscosity and infinite viscosity. A similar comparison is made in Fig. 14 for the elements of the viscosity tensor. For the $n=1$ mode, which corresponds to a shift of the center of mass, the Werner-Wheeler method gives trivially the exact results for both irrotational flow and infinite viscosity. For $n=2$, the Werner-Wheeler method gives the exact results for irrotational flow, but

for infinite viscosity it underestimates the inertia element by 5% and overestimates the viscosity element by 32%. For the higher modes, both the inertia elements and the viscosity elements calculated by use of the Werner-Wheeler method are larger than the values corresponding to either zero viscosity or infinite viscosity.

For pure spheroidal distortions of arbitrarily large eccentricity, the flow produced by the Werner-Wheeler method is exactly irrotational. In this case the inertia with respect to the semi-symmetry axis c of the spheroid is given by[14]

$$M_c = \tfrac{1}{5}[1 + \tfrac{1}{2}(R_0/c)^3]M_0 .$$

The corresponding element of the two-body viscosity tensor is[36]

$$\eta_c = 4\pi \frac{R_0^3}{c^2} \mu .$$

For the nearly spherical shapes for which an exact solution is possible in the presence of viscosity, fission is primarily an $n=2$ motion, with a small admixture of $n=4$ motion. From the above results and from considerations of the solutions for finite viscosity, we conclude that a value of the viscosity coefficient inferred from dynamical calculations in which the Werner-Wheeler method is used will be underestimated by roughly 30–50% if the viscosity is large enough to put the system in the region of the large-viscosity limit.

It should be stressed that the results in this appendix are valid only for small motions about a sphere. The fission mode corresponds to large-amplitude nonoscillatory motion in which large vorticities could be built up by moderate viscosity because the motion is unidirectional. This could cause the inertia and viscosity tensors to vary significantly from their small-oscillation values.

---

*This work was supported by the U. S. Energy Research and Development Administration under contracts with Union Carbide Corporation and the University of California.

[1]P. Bonche, S. E. Koonin, and J. W. Negele, Phys. Rev. C 13, 1226 (1976).

[2]S. E. Koonin, in Proceedings of the International Workshop IV on Gross Properties of Nuclei and Nuclear Excitations, Hirschegg, Kleinwalsertal, Austria, 1976 [Technische Hochschule Darmstadt Report No. AED-Conf-76-015-000, 1976 (unpublished)], p. 9; Phys. Lett. (to be published).

[3]R. Y. Cusson and J. Maruhn, Phys. Lett. (to be published).

[4]S. E. Koonin, Ph.D. thesis, Massachusetts Institute of Technology, 1975 (unpublished).

[5]C. Y. Wong, J. A. Maruhn, and T. A. Welton, Nucl. Phys. A253, 469 (1975).

[6]C. Y. Wong, T. A. Welton, and J. A. Maruhn, Oak Ridge National Laboratory report, 1975 (unpublished).

[7]C. Y. Wong, Oak Ridge National Laboratory report, 1975 (unpublished).

[8]C. Y. Wong, Lawrence Berkeley Laboratory report, 1975 (unpublished).

[9]C. Y. Wong, Oak Ridge National Laboratory Report No. ORNL-TM-5000, 1975 (unpublished).

[10]D. L. Hill and J. A. Wheeler, Phys. Rev. 89, 1102 (1953).

[11]D. L. Hill, in *Proceedings of the Second United Nations International Conference on the Peaceful Uses of Atomic Energy, Geneva, Switzerland, 1958* (United Nations, Geneva, 1958), Vol. 15, p. 244.

[12]C. T. Alonso, Lawrence Berkeley Laboratory Report No. LBL-2993, 1974 (unpublished).

[13]J. R. Nix, in *Proceedings of the Third Conference on Reactions between Complex Nuclei, Asilomar, California, 1963*, edited by A. Ghiorso, R. M. Diamond, and H. E. Conzett (Univ. of California Press, Berkeley, 1963), p. 366.

[14]J. R. Nix and W. J. Swiatecki, Nucl. Phys. 71, 1 (1965); J. R. Nix, Lawrence Berkeley Laboratory Report No. UCRL-11338, 1964 (unpublished).

[15]J. R. Nix, in *Contributions to the International Conference on Nuclear Structure, Tokyo, Japan, 1967* (University of Tokyo, Tokyo, 1967), p. 225.

[16]J. R. Nix, in Contributions to the International Symposium on Nuclear Structure, Dubna, U.S.S.R., 1968 [Joint Institute for Nuclear Research Report No. JINR-D-3893, 1968 (unpublished)], p. 85.

[17]J. R. Nix, Nucl. Phys. A130, 241 (1969); Lawrence Berkeley Laboratory Report No. UCRL-17958, 1968 (unpublished).

[18]J. R. Nix, in Proceedings of the Fifth Summer School on Nuclear Physics, Rudziska, Poland, 1972 [Institute of Nuclear Research Report No. INR-P-1447/I/PL, 1972 (unpublished)], Vol. 1, p. 299.

[19]A. J. Sierk and J. R. Nix, in *Proceedings of the Third International Atomic Energy Agency Symposium on the Physics and Chemistry of Fission, Rochester, New York, 1973* (International Atomic Energy Agency, Vienna, 1974), Vol. II, p. 273.

[20]J. R. Nix and A. J. Sierk, Phys. Scr. 10A, 94 (1974).

[21]K. T. R. Davies, S. E. Koonin, J. R. Nix, and A. J. Sierk, in Proceedings of the International Workshop III on Gross Properties of Nuclei and Nuclear Excitations, Hirschegg, Kleinwalsertal, Austria, 1975, edited by W. D. Myers [Technische Hochschule Darmstadt Report No. AED-Conf-75-009-000, 1975 (unpublished)], p. 8.

[22]A. J. Sierk and J. R. Nix, Los Alamos Scientific Laboratory report (unpublished).

[23]I. Kelson, Phys. Rev. 136, B1667 (1964).

[24]J. N. P. Lawrence, Los Alamos Scientific Laboratory Report No. LA-3774, 1967 (unpublished).

[25]R. W. Hasse, Phys. Lett. 27B, 605 (1968).

[26]R. W. Hasse, Nucl. Phys. A128, 609 (1969).

[27]R. W. Hasse, in *Proceedings of the Second International Atomic Energy Agency Symposium on the Physics and Chemistry of Fission, Vienna, Austria, 1969* (Interna-

tional Atomic Energy Agency, Vienna, 1969), p. 33.
[28]R. W. Hasse, Phys. Rev. C 4, 572 (1971).
[29]T. Ledergerber and H. C. Pauli, Phys. Lett. 39B, 307 (1972); Nucl. Phys. A207, 1 (1973).
[30]H. C. Pauli and T. Ledergerber, in *Proceedings of the Third International Atomic Energy Agency Symposium on the Physics and Chemistry of Fission, Rochester, New York, 1973* (see Ref. 19), Vol. I, p. 463.
[31]H. C. Pauli, Phys. Scr. 10A, 127 (1974).
[32]G. Wegmann, Phys. Lett. 50B, 327 (1974); in Proceedings of the International Workshop III on Gross Properties of Nuclei and Nuclear Excitations, Hirschegg, Kleinwalsertal, Austria, 1975 (see Ref. 21), p. 28.
[33]D. H. E. Gross, Nucl. Phys. A240, 472 (1975).
[34]W. J. Swiatecki, Lawrence Berkeley Laboratory Report No. LBL-4296, 1975 (unpublished).
[35]J. Blocki *et al.*, Lawrence Berkeley Laboratory report (unpublished).
[36]J. Schirmer, S. Knaak, and G. Süssmann, Nucl. Phys. A199, 31 (1973).
[37]R. Wieczorek, R. W. Hasse, and G. Süssmann, in *Proceedings of the Third International Atomic Energy Agency Symposium on the Physics and Chemistry of Fission, Rochester, New York, 1973* (see Ref. 19), Vol. I, p. 523.
[38]R. Wieczorek, R. W. Hasse, and G. Süssmann, in *Proceedings of the International Conference on Nuclear Physics, Munich, Germany, 1973,* edited by J. de Boer and H. J. Mang (North-Holland, Amsterdam/American Elsevier, New York, 1973), Vol. 1, p. 585.
[39]R. W. Hasse, in Proceedings of the International Workshop III on Gross Properties of Nuclei and Nuclear Excitations, Hirschegg, Kleinwalsertal, Austria, 1975 (see Ref. 21), p. 22.
[40]H. J. Krappe and J. R. Nix, in *Proceedings of the Third International Atomic Energy Agency Symposium on the Physics and Chemistry of Fission, Rochester, New York, 1973* (see Ref. 19), Vol. I, p. 159.
[41]H. J. Krappe, in *Proceedings of the Symposium on Classical and Quantum Mechanical Aspects of Heavy Ion Collisions, Heidelberg, Germany, 1974,* edited by H. L. Harney, P. Braun-Munzinger, and C. K. Gelbke (Springer-Verlag, Berlin, 1975), p. 24.
[42]F. G. Werner and J. A. Wheeler (unpublished).
[43]H. Goldstein, *Classical Mechanics* (Addison-Wesley, Reading, 1959), Chap. 1, Sec. 5, pp. 19–22.
[44]J. R. Nix, Annu. Rev. Nucl. Sci. 22, 65 (1972).
[45]K. T. R. Davies and A. J. Sierk, J. Comp. Phys. 18, 311 (1975).
[46]W. D. Myers and W. J. Swiatecki, Ark. Fys. 36, 343 (1967).
[47]W. D. Myers, Nucl. Phys. A204, 465 (1973).
[48]W. D. Myers, Lawrence Berkeley Laboratory Report No. LBL-3428, 1974 (unpublished).
[49]H. Goldstein, *Classical Mechanics* (see Ref. 43), Chap. 7, Sec. 1, pp. 215–218.
[50]L. P. Meissner, Lawrence Berkeley Laboratory Computer Center Program No. D2 BKY ZAM, 1965 (unpublished).
[51]J. A. Zonneveld, *Automatic Numerical Integration,* Mathematical Center Tract No. 8 (Mathematisch Centrum, Amsterdam, 1964), p. 23.
[52]S. E. Koonin (unpublished).
[53]P. Fong, *Statistical Theory of Nuclear Fission* (Gordon and Breach, New York, 1969).
[54]L. Wilets, *Theories of Nuclear Fission* (Clarendon, Oxford, 1964), Sec. 3.3.1, pp. 46–47.
[55]M. Bolsterli, E. O. Fiset, J. R. Nix, and J. L. Norton, Phys. Rev. C 5, 1050 (1972).
[56]A. Gavron, Phys. Rev. C 11, 580 (1975).
[57]A. Gavron and Z. Fraenkel, Phys. Rev. C 9, 632 (1974).
[58]S. Cohen and W. J. Swiatecki, Ann. Phys. (N.Y.) 22, 406 (1963).
[59]A. E. S. Green, *Nuclear Physics* (McGraw-Hill, New York, 1955), pp. 185, 250.
[60]B. Borderie, F. Hanappe, C. Ngô, J. Péter, and B. Tamain, Nucl. Phys. A220, 93 (1974).
[61]J. Galin, M. Lefort, J. Péter, X. Tarrago, E. Cheifetz, and Z. Fraenkel, Nucl. Phys. A134, 513 (1969).
[62]H. C. Britt, H. E. Wegner, and J. C. Gursky, Phys. Rev. 129, 2239 (1963).
[63]F. Plasil, D. S. Burnett, H. C. Britt, and S. G. Thompson, Phys. Rev. 142, 696 (1966).
[64]T. Sikkeland, Phys. Lett. 31B, 451 (1970).
[65]D. S. Burnett, Lawrence Berkeley Laboratory Report No. UCRL-11006, 1963 (unpublished).
[66]M. N. Namboodiri, J. B. Natowitz, E. T. Chulick, K. Das, and L. Webb, Nucl. Phys. A252, 163 (1975).
[67]C. Cabot, C. Ngô, J. Péter, and B. Tamain, Nucl. Phys. A244, 134 (1975).
[68]J. Barrette, P. Braun-Munzinger, C. K. Gelbke, E. Grosse, H. L. Harney, J. Kuzminski, I. Tserruya, and Th. Walcher, Z. Phys. A274, 121 (1975).
[69]V. E. Viola, Jr., and T. Sikkeland, Phys. Rev. 130, 2044 (1963).
[70]V. E. Viola, Jr., Nucl. Data A1, 391 (1966).
[71]T. Sikkeland, Phys. Lett. 27B, 277 (1968). Misprint: the experimental kinetic energy should be 225±4 MeV rather than 255±4 MeV.
[72]F. Plasil, R. L. Ferguson, and F. Pleasonton, in *Proceedings of the Third International Atomic Energy Agency Symposium on the Physics and Chemistry of Fission, Rochester, New York, 1973* (see Ref. 19), Vol. II, p. 319.
[73]H. Goldstein, *Classical Mechanics* (see Ref. 43), Chap. 1, Sec. 6, pp. 22–23.
[74]K. R. Symon, *Mechanics* (Addison-Wesley, Reading, 1971), 3rd ed., Chap. 8, Sec. 6, pp. 313–320.
[75]H. Lamb, *Hydrodynamics* (Dover, New York, 1945), 6th ed., Sec. 329, pp. 579–581.
[76]H. Lamb, *Hydrodynamics* (see Ref. 75), 6th ed., Sec. 45, pp. 47–48.
[77]H. Lamb, Proc. Lond. Math. Soc. 13, 51 (1881).
[78]S. Chandrasekhar, Proc. Lond. Math. Soc. 9, 141 (1959).
[79]W. H. Reid, Q. Appl. Math. 18, 86 (1960).
[80]H. H. K. Tang and C. Y. Wong, J. Phys. A 7, 1038 (1974).
[81]R. W. Hasse, Ann. Phys. (N.Y.) 93, 68 (1975).
[82]J. R. Nix, Ann. Phys. (N.Y.) 41, 52 (1967).
[83]For the $n=2$, 3, and 4 modes in the limit of infinite two-body viscosity the inertia is therefore 105%, 112%, and 117%, respectively, of the irrotational values, whereas the viscosity is 76%, 67%, and 63%, respectively, of the irrotational values. The corresponding results listed in the appendix of Ref. 19 are slightly incorrect.
[84]This result is contained implicitly in H. Lamb, *Hydro-*

dynamics (see Ref. 75), 6th ed., Sec. 355, p. 641, Eq. (15).

[85]I. S. Gradshteyn and I. M. Ryzhik, *Tables of Integrals, Series, and Products*, prepared by Yu. V. Geronimus and M. Yu. Tseytlin, translation edited by A. Jeffrey (Academic, New York, 1965), 4th ed., Sec. 8.81, pp. 1014–1016.